SINGLE IONIZATION OF He BY HIGH-ENERGY PROTON AND ANTIPROTON. A QED APPROACH

S. BHATTACHARYYA* AND K. PATHAK

Department of Physics, Gokhale Memorial Girls' College, Calcutta — 700020, India

(Received March 24, 2000; revised version July 17, 2000)

We have investigated single ionization of He by fast proton and antiproton using a QED approach. A field theoretical calculation gives the total cross-section of He in single ionization, from which it is seen that the projectile p^+ or p^- gives almost the same values of cross-section. We have also compared our results with other theoretical and experimental results available in this context yet. Behaviour of the cross-section at a lower spectrum of projectile energy is discussed.

PACS numbers: 34.80.Dp, 82.30.Fi

1. Introduction

A QED approach is previously applied in many atomic collision problems by the first author (Bhattacharyya) and her group [1–4]. In this paper we have studied the phenomenon of single ionization (SI) of He by proton (p^+) and antiproton (p^-) from the quantum electrodynamic [5] point of view. The reaction under consideration

$$p^+(p^-) + He \rightarrow p^+(p^-) + He^+ + e^- \tag{1}$$

can be represented by the second order Feynman diagram [6] with one virtual photon exchange between the projectile and one of the bound electrons [7].

Single ionization (SI) is previously calculated by Voitkiv [8] due to soft collisions of fast highly charged ions with H, He atoms. Reading, Bronk, and Ford [9] discussed electron–electron correlation in ionization of He by high-energy p^+ and p^-. Ford and Reading [10] used the forced impulse method (FIM) to calculate SI and double ionization (DI) of He by high-energy proton and antiproton. Fainstein et al. [11] used continuum distorted wave eikonal initial state model to study SI of He by p^+, p^-, He^{2+}, and Li^{3+}. Shah and Gilbody [12] measured SI of He by proton. Hvelfund et al. [13] have done the same with antiproton. Anderson et al. [14] have obtained the resuls on SI both experimentally and theoretically. Ben-Itzhak

*corresponding author, e-mail: sbgcmr@cal2.vsnl.net.in

et al. [15] have measured SI cross-section of H and He by proton and antiproton. However, the experimental results and theoretical calculations differ among themselves. Since the study of single ionization of a two-electron target has not been yet completed we like to apply a field theoretic approach to calculate the cross-section for reaction (1). Recently the field theoretic technique has been successfully applied to explain the bound state problems like ionization–excitation [2], charge transfer [3], photoionization [1], etc. We are tempted to use the technique on SI in this paper. The present result is compared with the existing theoretical and experimental results. For projectile energy above 1 MeV fair agreement is obtained.

2. Mathematical formulation

We have computed the second order S-matrix for SI of He by proton and antiproton in the energy range of 0.1 to 2 MeV. At such high energies the interaction time is much shorter than the orbital rotation time. The high-energy projectile interacts with the electron cloud of the He atom ejecting one of the electrons and leaving behind He^+ in the ground state. The phenomenon is, like scattering of an electron by a charged projectile, due to the interaction between a localized electron and a high-energy projectile. The Mott scattering diagram of Feynman (Fig. 1) is the nearest approach to such a phenomenon of SI in the QED model. Although we restrict ourselves to the second order S-matrix corresponding to the lowest order perturbation theory with regard to radiation field (one virtual photon exchange), we can obtain results accurate to all orders in Coulomb coupling by a suitable choice of the wave functions. The Sommerfeld–Maue relativistic wave function is well suited to describe the incoming distorted wave projectile. To estimate the effect of this additional Coulomb coupling over the second order S-matrix

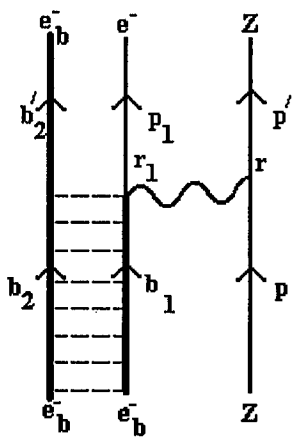

Fig. 1. Feynman diagram for single ionization of He. Z is the projectile charge, e_b^- and e^- represent bound and ionized electrons, respectively. Wavy line and broken line represent virtual and Coulomb photon exchanges, respectively.

particle-radiation-field coupling we can multiply the cross-section by the Sommerfeld factor [3].

2.1. Interaction terms

To calculate the single ionization cross-section we define the following terms: Let $p(p_0, p)$ and $p'(p'_0, p')$ be the four-momenta (Fig. 1) of the projectile before and after interaction, respectively. $b_1(b_{10}, 0)$ and $b_2(b_{20}, 0)$ be the four-momenta of the two target electrons. The four-momenta of the ionized electron after ionization is $p_1(p_{10}, p_1)$, while that of the second bound electron will remain the same as $b_2(b_{20}, 0)$.

The S-matrix S_{SI} for SI is obtained in a similar way as done in [3] for the shake-up (SU) term S_{su}. The difference between SU and SI is that the second electron at r_2 in the former case gets excited (see Eq. (3a) of [3]) while in the later case that electron remains in the ground state. Eventually the interaction term S_{SI} from the Feynman diagram (Fig. 1) is

$$S_{\mathrm{SI}} = Ze^2 \int [J_\nu(p, p')]_r D(r - r_1)[J'_\mu(p_1, b_1)]_{r_1}$$

$$\times C^+_{b_2} \overline{V}(b_2, r_2) C_{b_2} V(b_2, r_2) \mathrm{d}^4 r_2 \mathrm{d}^4 r_1 \mathrm{d}^4 r, \tag{2}$$

$[J_\nu(p, p')]_r$ is the projectile four-current at r; $[J'_\mu(p_i, b_i)]_{r_1}$ is the four-current at r_1 with the initial bound-electron line and the final free-electron line (Fig. 1); $D(r - r_1)$ is the virtual photon propagator between the projectile and one of the target electrons. Necessary expressions [3] for these terms are shown in the Appendix (A1–A4).

Let $|\psi_{\mathrm{i}}\rangle$ and $|\psi_{\mathrm{f}}\rangle$ be the state vectors for the interacting system of particles in the initial and in the final states, respectively. Taking $\phi_{\mathrm{i}}(x, y, R)$ as the solution of the Schrödinger equation for the interacting system in the initial state and $\phi_{\mathrm{f}}(x, y, R)$ as that for the final state, and C's and a's as the annihilation operators for the projectile and electron, respectively, the state vectors become [3]

$$|\psi_{\mathrm{i}}\rangle = (2\pi)^{-1/2} \exp(-\mathrm{i} R_0 L_0) \phi_{\mathrm{i}}(x, y, R) C^+_{b_1} C^+_{b_2} a^+_p |0\rangle, \tag{3}$$

$$|\psi_{\mathrm{f}}\rangle = (2\pi)^{-1/2} \exp(-\mathrm{i} R_0 L'_0) \phi_{\mathrm{f}}(x, y, R) C^+_{p_1} C^+_{b_2} a^+_{p'} |0\rangle, \tag{4}$$

L_0 and L'_0 represent the energy components of the centre-of-mass (CM) of four-momenta $L(L_0, \boldsymbol{L})$ and $L'(L'_0, \boldsymbol{L'})$, respectively; R_0 is the time component of the four-coordinate $R(R_0, \boldsymbol{R})$ of the CM. Let r_1, r_2 be the space coordinates of the two bound electrons and $\boldsymbol{R}$ be the coordinate of the CM of the He atom from an arbitrary origin. In the CM and relative coordinates, the unperturbed solution of the Schrödinger equation for He atom is

$$\Phi_{\mathrm{i}}(x, y, R) = (2\pi)^{-3/2} \exp(\mathrm{i} \boldsymbol{R} \boldsymbol{L}) \Phi_{1s^2}(x, y), \tag{5}$$

where

$$\boldsymbol{x} = \boldsymbol{r}_1 - \boldsymbol{R}, \qquad \boldsymbol{y} = \boldsymbol{r}_2 - \boldsymbol{R}, \tag{6}$$

$\Phi_{1s^2}(x, y)$ — the correlated wave function [19] of the He atom in the ground state is given in the Appendix Eq. (A5).

For fast collision, under consideration, with high-energy projectile, the momentum transfer is usually small and the projectile trajectory hardly deviates from the projectile beam direction. Eventually, the SI is dominated by low energy ejected electrons. The final wave function of the interacting system of He^+ and the ionized electron is given by

$$\phi_f(x, y, R) = (2\pi)^{-3/2} F_C(p_1) \exp(i\boldsymbol{R}\boldsymbol{L}')\phi'_f(x, y), \tag{7}$$

where

$$\phi'_f(x, y) = (1/\sqrt{2})[\phi(y) + \phi(x)], \tag{8}$$

$F_C(p_1)$ is the Coulomb distortion factor (A6) to the plane wave of the ejected electron, $\phi(x)$ and $\phi(y)$ are the wave functions of the bound electron in the He^+ state as given in Eq. (A7).

2.2. The amplitude

The amplitude M_{SI} is obtained after operating the interaction term S_{SI} between the initial state $|\psi_i\rangle$ and the final state $|\psi_f\rangle$

$$M_{SI} = \langle\psi_f|S_{SI}|\psi_i\rangle. \tag{9}$$

After some lengthy calculations as shown in the Appendix (A8–A10) the amplitude becomes

$$M_{SI} = (2\pi)^{-10}\sqrt{2\pi}Ze^2\overline{C}\delta(E_i - E_f)$$
$$\times(2\pi)^3\delta^3(\boldsymbol{L}' - \boldsymbol{L} + \boldsymbol{p}' - \boldsymbol{p} + \boldsymbol{p}_1)I(p' - p)^{-2}. \tag{10}$$

The overlap integral

$$I = \int \phi_{1s^2}(x, y)\phi'_f(x, y) \exp[i\boldsymbol{R}(\boldsymbol{L}' - \boldsymbol{L})]$$
$$\times \exp[ir_1(\boldsymbol{p}' - \boldsymbol{p} + \boldsymbol{p}_1)]d^3r_1 d^3y d^3\boldsymbol{R}. \tag{11}$$

Writing $K'' = (1/\sqrt{2})(2\pi e^2 m/|p_1|)^{1/2}$ and the recoil momentum $\boldsymbol{K} = \boldsymbol{p}' - \boldsymbol{p} - \boldsymbol{p}_1$, the overlap integral (A12) becomes

$$I = 2K''(8\pi)^2\left(\frac{a}{ak} + \frac{\alpha' + a}{bk} + \frac{b}{ck} + \frac{\alpha' + b}{dk}\right), \tag{12}$$

where

$$ak = (\alpha' + b)^3(a^2 + |\boldsymbol{K}|^2)^2, \qquad bk = b^3[(\alpha' + a)^2 + |\boldsymbol{K}|^2]^2,$$

$$ck = (\alpha' + a)^3(b^2 + |\boldsymbol{K}|^2)^2 \text{ and } dk = a^3[(\alpha' + b)^2 + |\boldsymbol{K}|^2]^2.$$

2.3. Total cross-section

The phase space for SI and the incident flux are respectively $d^3p' d^3p_1/(2\pi)^6$ and $M/|\boldsymbol{p}|$, and writing the amplitude $M_{SI} = M_{fi}^Z$ the total cross-section for single ionization becomes

$$\sigma_{SI} = (2\pi)^{-6}\frac{M}{|\boldsymbol{p}|}\int |M_{fi}^Z|^2 d^3p' d^3p_1, \tag{13}$$

where from (A9)

$$\left|M_{\mathrm{fi}}^{Z}\right|^{2} = (2\pi)^{-15}(Ze^{2})^{2}[\delta^{4}(p_{\mathrm{i}} - p_{\mathrm{f}})]\overline{C}^{2}(p' - p)^{-4}I^{2}. \tag{14}$$

Using the energy and momentum conservation law the four-momentum transfer is

$$(p' - p)^{2} = (p'_{0} - p_{0})^{2}(\boldsymbol{p}' - \boldsymbol{p})^{2} = (E_{1} + \varepsilon_{1s})^{2}(\boldsymbol{p}_{1} + |\boldsymbol{K}|)^{2}.$$

Using (A13, A14), and after integrating the momentum delta function over $\mathrm{d}^{3}p'$ the cross-section (13) becomes

$$\sigma_{\mathrm{SI}} = (2\pi)^{-20}(M/|\boldsymbol{p}|)(Ze^{2})^{2}(1/2)(1 + m/M)$$
$$\times \int [(E_{1} + \varepsilon_{1s})(\boldsymbol{p}_{1} + \boldsymbol{K})]^{-4}I^{2}(2mE_{1})^{1/2}m\mathrm{d}E_{1}\sin\theta_{1}\mathrm{d}\theta_{1}. \tag{15}$$

3. Results and discussions

The cross-section is computed for the projectile energy range of 0.1 to 2 Mev. At such high-energy collisions the interaction time is much shorter than the orbital rotation time, and the bound electron behaves like a free particle relative to the projectile. The Feynman diagram is the same as that for the usual Mott scattering diagram between two charged particles. The bound character of the initial electron comes through its wave function. In the present computation the recoil of the target is negligible and the high-energy projectile moves almost in the forward direction with little loss of momentum. The maximum contribution to the cross-section comes from the electrons ejected with the energy E_1 such that $0 < E_1 < \varepsilon_{1s}$. As the recoil momentum $\boldsymbol{K}$ becomes negligible, the overlap integral I (12) becomes independent of the projectile velocity but depends inversely on the square root of the ejected electron velocity. Further when the projectile kinetic energy is less than its rest mass, the factor $\overline{C}^{2}$ (A11, A15) containing the trace part $|T_3T_1|^2$ and the normalization factor D_eD_z becomes a c-number. As such the single ionization cross-section (15) varies inversely with the projectile momentum, contributed by the incident flux. Thus the single ionization cross-section decreases with the increase in the projectile energy. The present result compares well with the experimental data and other theoretical predictions (Table) for the projectile energy range from 0.5 MeV onwards. From (15) we find that the cross-section σ_{SI} carries a square of the projectile charge. Eventually, the value of the amplitude and hence the cross-sections remain the same for single ionization of He by proton and antiproton.

3.1. Low energy behaviour

Below 0.5 MeV the higher value of the present cross-section relative to the experimental results may be due to the choice of the Coulomb distortion factor which needs to be more exact in the low energy range to dampen the cross--section. Further, from the physical point of view at low velocities the projectile cloud may penetrate the electron orbit of the atom to interact with the atomic core. This results in the change in the Coulomb field of the nucleus effecting the electron–electron correlation, and causing the ejection of an electron. This is

TABLE

Single ionization cross-sections (SICS) in units of 10^{-17} cm^2 and corresponding projectile energies E in MeV from the present field theoretic (FT) calculation and from other theoretical and experimental results.

Present FT results		Anderson et al. [14] Theoretical results			Experimental results by					
					Shah & Gilbody [12]		Anderson et al. [14]		Hvelplund et al. [13]	
E	SICS p^+ and p^-	E	SICS (p^+)	SICS (p^-)	E	SICS (p^+)	E	SICS (p^-)	E	SICS (p^-)
0.1	31.93	0.3	5.0	4.5	0.166	7.5	0.2	5.6	0.16	6.25
0.3	11.01	0.4	4.12	3.8	0.2	6.8	0.3	5.0	0.175	5.275
0.5	4.53	0.5	3.5	3.3	0.266	5.8	0.4	4.0	0.2	5.25
0.7	2.5	0.6	3.0	2.8	0.3	5.12	1.2	1.9	0.275	4.66
1.1	1.44	0.8	2.5	2.4	0.425	4.33	1.6	1.75	0.5	3.5
1.3	1.17	1.0	2.12		0.625	3.11	1.9	1.25		
1.5	0.99	1.5	1.5		0.8	2.66	2.5	1.0		
1.9	0.766	2.0	1.25		1.0	2.25	3.0	1.0		
					2.0	1.25				

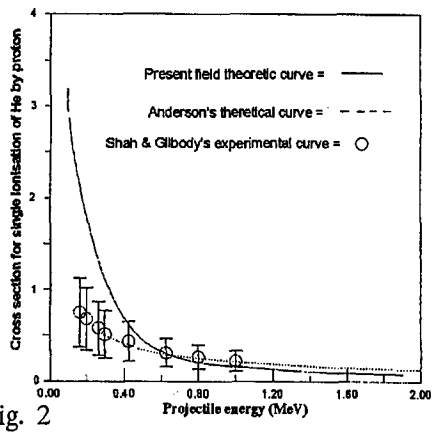

Fig. 2

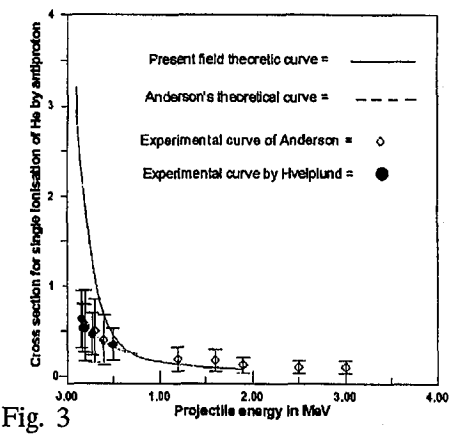

Fig. 3

Fig. 2. Cross-section (10^{-16} cm^2) for single ionization of He by proton versus projectile energy.

Fig. 3. The same as in Fig. 2 by antiproton.

the projectile-nucleus interaction term. Contributions from the projectile-nucleus term, the projectile-bound-electron term (S_{SI}), and interference between these two terms may have a significant effect on the cross-section in the energy range below 0.5 MeV. In principle, due to the projectile-nucleus term, SI cross-section by positive projectile may be different from that by the negative projectile. Hopefully, the above scenario explains the difference between the experimental and the

present theoretical results below 0.5 MeV. This low energy behaviour requires a separate calculation and will be taken up in the future. The present QED results and experimental results of Shah and Gillbody, along with the theoretical results of Anderson are given in the Table [1], Figs. 2 and 3.

4. Conclusions

We have given an analytical expression for single ionization of He by proton and antiproton in a QED technique using the Feynman diagram. In the high-energy collision since the interaction time is much smaller than the orbital rotation time the electron cloud round the nucleus behaves as free electron cloud relative to the projectile. The presence of nucleus is felt through the bound wave function of the electron. Thus a second-order Feynman diagram is the nearest approach to the phenomena of single ionization in the high-energy limit. In the high-energy region, the projectile current at the vertex r in the second-order Feynman diagram (Fig. 1) has a factor Z (projectile charge). Hence, the cross-section which contains Z^2, becomes independent of signs of the projectile charge. However, in the low-energy region we need to consider the projectile-nucleus interaction diagram along with the more exact Coulomb distortion effect for calculating the cross-section. This may further cause a change in the cross-section by positive and negative projectile in the low-energy limit. In conclusion we like to say that the present field theoretic result agrees in principle with the existing experimental results and theoretical predictions in the high-energy limit.

Appendix

Taking $U(p)$ and a_p as the Dirac spinor and the annihilation operator, respectively, for the charged projectile, corresponding four-current at r in Fig. 1 is

$$[J_\nu(p,p')]_r = \left(\frac{M^2}{E_p^R E_{p'}^R}\right)^{1/2} (2\pi)^{-3} \exp\left[\mathrm{i}(p'-p)r\right]$$

$$\times \sum_n [\overline{U}_n(p')\gamma U_n(p)] a_{p'}^+ a_p, \tag{A1}$$

M is the projectile mass and, $E_p^R(=p_0)$ and $E_{p'}^R(=p_0')$ are the relativistic energies of the particles with suffixed momenta.

C_{p_1} and $u(p_1)$ are the annihilation operator and the Dirac spinor, respectively for an electron with momentum $p_1(p_{10}, p_I)$. The Dirac spinor for a bound electron [2] is

$$V(b_i, r_i) = \left[1 - \frac{1}{2}\alpha\xi\gamma_4(\gamma\cdot n)\right](2\pi)^{-3/2} U(b_i)\exp\left(-\mathrm{i}b_i r_i\right), \tag{A2}$$

where $n = r_\mathrm{i}/|r_\mathrm{i}|$, $\alpha = 1/137$, $\xi =$ target nuclear charge, and $U(b_i)$ is the Dirac spinor for a free electron with the momentum b_i. The four-current at r_i with the initial bound-electron line and the final free electron line (Fig. 1) is

$$[J'_\mu(p_i,b_i)]_{r_1} = \left(\frac{m}{E^R_{p_i}}\right)^{1/2}(2\pi)^{-3/2}\exp(\mathrm{i}p_i r_i)$$

$$\times \sum_x [\overline{U}_x(p_i)\gamma_\mu V_x(b_i,r_1)]C^+_{p_i}C_{b_i}, \tag{A3}$$

where $E^R_{p_1} = p_{10}$. The virtual photon propagator between the projectile and one of the target electrons (Fig. 1) is

$$D(r-r_1) = \int (2\pi)^{-4}(q_1^2+\mathrm{i}\varepsilon)^{-1}\exp[\mathrm{i}q_1(r_1-r)]\mathrm{d}^4q_1. \tag{A4}$$

The wave function of He($1s^2$) [19] is

$$\phi_{1s^2}(x,y) = N\left(\mathrm{e}^{-ax}\mathrm{e}^{-by} + \mathrm{e}^{-bx}\mathrm{e}^{-ay}\right). \tag{A5}$$

Taking the Coulomb distortion factor as

$$F_C(p_1) = (2\pi e^2 m/|p_1|)^{1/2} \tag{A6}$$

and

$$\phi(x) = N'\mathrm{e}^{-\alpha' x}, \quad \alpha' = 2(Z/a_0), \tag{A7}$$

$$M_{SI} = \langle\psi_f|S_{SI}|\psi_i\rangle = (2\pi)^{-25/2}Ze^2GD_Z D_e T_3 T_1$$

$$\times \int \exp(\mathrm{i}R_0)(L'_0 - L_0)(q^2+\mathrm{i}\varepsilon)^{-1}\exp[\mathrm{i}r(p'-p)+\mathrm{i}q(r_1-r)$$

$$+ r_1(p_1-b_1)]\,\phi_f(x,y,R)\phi_i(x,y,R)\mathrm{d}^4q\mathrm{d}^4r\mathrm{d}^4r_1\mathrm{d}^4R. \tag{A8}$$

After integration over r, q, and R_0, M_{SI} becomes

$$M_{SI} = (2\pi)^{-8}(2\pi)^{3/2}Ze^2GD_Z D_e T_3 T_1$$

$$\times \int (p'-p)^{-2}\delta(L'_0 - L_0 + p'_0 - p_0 + p_{10} - b_{10})(2\pi)^{-3}$$

$$\times \exp[\mathrm{i}\boldsymbol{R}(\boldsymbol{L}'-\boldsymbol{L})]\phi_{1s^2}(x,y)\phi'(x,y)\exp[\mathrm{i}r_1(\boldsymbol{p}'-\boldsymbol{p}+\boldsymbol{p}_1)]\mathrm{d}^3r_1\mathrm{d}^3\boldsymbol{R}. \tag{A9}$$

The vacuum expectation value G is given by

$$G = \langle 0|C_{b_1}C_{p_1}a_{p'}a^+_{p'}a_p C^+_{p_1}C_{b_1}a^+_p C^+_{b_1}C^+_{b_2}|0\rangle = 1.$$

The spinor parts T_3, T_4, and D's are given by

$$T_3 = \overline{U}(p')\gamma_\mu U(p),$$

$$T_1 = \overline{u}(p_1)\gamma_\nu u(b_1),$$

$$D_Z = \left(\frac{M^2}{E^R_{p'_0}E^R_{p_0}}\right)^{1/2}, \quad p'_0 = E^R_{p'_0}, \quad p_0 = E^R_{p_0},$$

$$D_e = \left(\frac{M}{E^R_{p_{10}}E^R_{b_{10}}}\right)^{1/2}, \quad p_{10} = E^R_{p_{10}}, \quad b_{10} = E^R_{b_{10}}.$$

The overlap integral

$$I = \int \phi_{1s^2}(x,y)\phi'(x,y)\exp[\mathrm{i}\boldsymbol{R}(\boldsymbol{L}'-\boldsymbol{L})] \times \exp[\mathrm{i}r_1(\boldsymbol{p}'-\boldsymbol{p}+\boldsymbol{p}_1)]\mathrm{d}^3r_1\mathrm{d}^3y\mathrm{d}^3\boldsymbol{R} \tag{A10}$$

and

$$\overline{C} = D_Z D_e T_3 T_1. \tag{A11}$$

On transforming the variable r_1 into $\boldsymbol{x}$ with the help of (6), the overlap integral I in (A10) becomes

$$I = \delta^3(\boldsymbol{L}'-\boldsymbol{L}+\boldsymbol{p}'-\boldsymbol{p}+\boldsymbol{p}_1)\int \phi'(x,y)\phi_{1s^2}(x,y) \times \exp[\mathrm{i}\boldsymbol{x}(\boldsymbol{p}'-\boldsymbol{p}+\boldsymbol{p}_1)]\mathrm{d}^3x\mathrm{d}^3y. \tag{A12}$$

Substituting (A5) and (A7) in (A12) we have

$$I = (1/\sqrt{2})(2\pi e^2 m/|\boldsymbol{p}_1|)^{1/2}N'N\delta^3(\boldsymbol{L}'-\boldsymbol{L}+\boldsymbol{p}'-\boldsymbol{p}+\boldsymbol{p}_1) \times \int (\mathrm{e}^{-a'y}+\mathrm{e}^{-a'x})(\mathrm{e}^{-ax-by}+\mathrm{e}^{-ay-bx}) \times \exp[\mathrm{i}\boldsymbol{x}(\boldsymbol{p}'-\boldsymbol{p}+\boldsymbol{p}_1)]\mathrm{d}^3x\mathrm{d}^3y \tag{A13}$$

and we get for the cross-section

$$\sigma_{\mathrm{SI}} = (2\pi)^{-6}(M/|\boldsymbol{p}|)(2\pi)^{-15}(Ze^2)^2\overline{C}^2 \times \int [(E_1+\varepsilon_{1s})^{-4}(\boldsymbol{p}_1+\boldsymbol{K})^{-4}]\, I^2\mathrm{d}^3p_1, \tag{A14}$$

where

$$\overline{C}^2 = (D_Z D_e)^2|T_3T_1|^2 = |T_3T_1|^2, \tag{A15}$$

$$(D_Z D_e) \approx 1, \quad |T_3T_1|^2 = (1/2)(1+m/M). \tag{A16}$$

Acknowledgment

The work is supported by UGC, New Delhi, through the project No. F10-17/98 (SR-I).

References

[1] S. Bhattacharyya, S. Mitra, *Phys. Rev. A* **60**, 2269 (1999); *Phys. Rev. A* **62**, 32709 (2000).

[2] S. Bhattacharyya, K. Pathak, *Phys. Scr.* **54**, 143 (1996).

[3] S. Bhattacharyya, K. Rinn, E. Salzborn, L. Chatterjee, *J. Phys. B* **21**, 111 (1988).

[4] S. Bhattacharyya, *Phys. Scr.* **42**, 159 (1990).

[5] A.I. Akhizer, V.B. Berestetsky, *Quantum Electrodynamics*, N.Y. Interscience, New York 1965, ch. 4, 5.

[6] S.S. Schweber, *An Introduction to Relativistic Quantum Field Theory*, Harper International Edition, Harper & Row Publishers, Tokyo 1966, ch. 4, 14.

[7] J.D. Bjorkrn, S.D. Drell, *Relativistic Quantum Mechanics*, McGraw Hill Book Company, New York 1964, p. 284.

[8] A.B. Voitkiv, *J. Phys. B, At. Mol. Phys.* **29**, 5433 (1996).

[9] J.F. Reading, T. Bronk, A.L. Ford, *J. Phys. B, At. Mol. Phys.* **29**, 6075 (1996).

[10] A.L. Ford, J.F. Reading, *J. Phys. B, At. Mol. Opt. Phys.* **27**, 4215 (1994).

[11] P.D. Fainstein, R.D. Ponce, V.H. Rivorola, *Phys. Rev. A* **36**, 3639 (1987).

[12] M.B. Shah, H.B. Gilbody, *J. Phys. B, At. Mol. Phys.* **18**, 899 (1985).

[13] P. Hvelplund, H. Knudsen, U. Mikkelsen, E. Morenzoni, S.P. Møller, E. Uggerhøj, T. Worm, *J. Phys. B, At. Mol. Opt. Phys.* **27**, 925 (1994).

[14] L.H. Anderson, P. Hvelplund, H. Knudsen, S.P. Møller, J.O.P. Pedersen, S. Tang-Petersen, E. Uggerhøj, K. Elsner, E. Morenzoni, *Phys. Rev. A* **40**, 7366 (1989).

[15] I. Ben-Itzhak, Vidya Krishnamurthy, K.D. Carnes, H. Aliabadi, H. Knudsen, U. Mikkelsen, *Nucl. Instrum. Methods in Phys. Res. B* **99**, 104 (1995).